Optical radiative crosstalk in integrated photonic waveguides

Daniele Melati,* Francesco Morichetti, Gian Guido Gentili, and Andrea Melloni

Dipartimento di Elettronica, Informazione e Bioingegneria, Politecnico di Milano, via Ponzio 34/5, 20133 Milano, Italy
**Corresponding author: daniele.melati@polimi.it*

Received April 24, 2014; revised May 26, 2014; accepted May 26, 2014;
posted May 27, 2014; published June 27, 2014

Photonic technologies are facing a pressing demand toward footprint reduction of single integrated components and a higher density of devices per chip [1]. However, a higher integration scale poses serious problems in the mutual interference (crosstalk) between different components on the chip, which can compromise the correct functionality of the complete circuit [2]. Among the different sources of crosstalk, unwanted optical power exchange between ideally uncoupled waveguides can directly limit the performance of any passive or active photonic component [3]. This effect is particularly detrimental for technologies that aim at very large-scale integration, such as plasmonic-waveguide-based devices [4] or high-index-contrast technologies for dielectric components. Since sidewall roughness represents the main source of power leakage by radiation for classical waveguides [5], part of the scattered light can reach a nearby waveguide and be coupled into one of its guided modes, generating optical crosstalk [6]. After the early analyses by Marcuse [6], scattering-induced optical crosstalk generally has been considered negligible; to the best of the authors' knowledge, no experimental evidence of its characteristics have been provided.

In this Letter, we report on the properties of roughness-induced radiative optical crosstalk on a photonic chip through an extensive experimental characterization of closely spaced passive waveguides. Our results show that as the gap distance between waveguides increases, a radiative coupling regime emerges, in which the power transfer between waveguides decreases with a power-law dependence on the gap distance and largely dominates the exponentially decaying evanescent coupling. An in-depth investigation on the nature of the roughness-induced optical crosstalk also reveals a phase decorrelation between the modes propagating in the radiatively coupled waveguides, as well as the excitation of higher-order modes.

Dedicated test structures were designed and fabricated to allow direct observation of radiative optical crosstalk. As shown in Fig. 1, the device concept consists of an S-shaped waveguide (between ports A and B, hereinafter referred to as direct waveguide) with a second 3-mm-long straight waveguide (terminating at port C, adjacent waveguide) running parallel at a distance g. Several structures were fabricated with g spanning 2–30 μm. The radius of the bent sections is 480 μm, sufficiently large to avoid bending losses and higher order mode excitation. The distance between output ports B and C is 30 μm for all the fabricated devices, irrespective of g, to minimize unwanted light coupling from the direct waveguide to the output fiber. The S-shaped layout reduces the impact of the stray light generated by the input fiber at port A on the light collected at port C of the adjacent waveguide. The optical waveguide, with a cross-section schematically shown in Fig. 1, was fabricated on an InP photonic platform. The shallow-etched rib geometry [7] has an InGaAsP core with a thickness of 1 μm that is laterally shaped by a 600 nm etch depth. The width of the waveguides is 2 μm. The substrate is composed of InP, resulting in a vertical index contrast $\Delta n = (n_{\mathrm{core}} - n_{\mathrm{sub}})/n_{\mathrm{sub}}$ of about 2.8%.

Crosstalk power was evaluated by comparing the power P_{xt} outgoing from port C of the adjacent waveguide to the power P_{out} collected at port B of the direct waveguide. Figure 2 shows the normalized power $\langle P_{\mathrm{out}}/(P_{\mathrm{out}} + P_{\mathrm{xt}})\rangle$ (blue crosses) and $\langle P_{\mathrm{xt}}/(P_{\mathrm{out}} + P_{\mathrm{xt}})\rangle$ (red dots), averaged across a 40-nm-wide wavelength

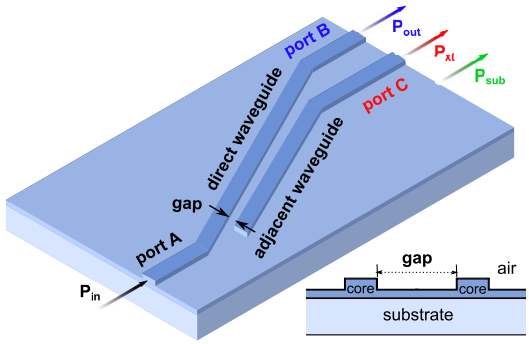

Fig. 1. Test structure for the measurement of optical radiative crosstalk with the cross-section of the InP rib-shaped waveguides in the lower right corner.

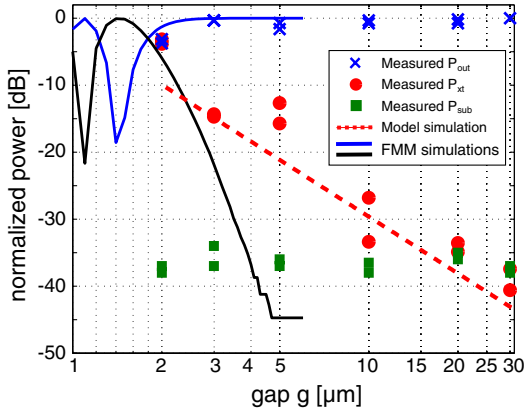

Fig. 2. Power coupling as function of the distance g between neighboring straight waveguides. The power at the output of the direct (P_{out}, blue crosses) and adjacent (P_{xt}, red dots) waveguides was experimentally measured and compared to simulated evanescent coupling contribution for perfectly smooth sidewalls (blue and black solid lines). A power-law dependence of the power crosstalk on the waveguide distance can be observed for a gap wider than 3 μm—behavior also confirmed by the developed model (red-dashed line).

range centered at 1.55 μm, as a function of the gap g for TE input light. Very similar results were obtained for the TM input polarization. The measured crosstalk drops from –3 dB for $g = 2$ μm to about –40 dB for $g = 30$ μm.

Depending on the gap g, different coupling regimes can be observed. At small g, evanescent field coupling dominates the power transfer between the two waveguides. Evanescent coupling was simulated (solid lines) in the absence of sidewall roughness by using a simulator (FIMMWAVE) based on a full-vectorial film mode matching technique [8] and properly explains the –3 dB power transfer measured at $g = 2$ μm. However, at larger g, the measured power coupling largely exceeds the results of numerical simulations. For $g \geq 5$ μm, a significant crosstalk power P_{xt} was measured at the output port C, while evanescent coupling should completely disappear. In this regime, therefore, a pure radiative coupling mechanisms occurs, induced by sidewall roughness [6]. For $g = 3$ μm, measurements show a power coupling 5 dB higher than the simulated evanescent coupling, suggesting an intermediate regime in which radiative effects play a significant role in the coupling mechanism.

The presence of substrate modes excited at the input section and propagating in the slab below the waveguides limits the dynamic range of the measurement to about 40 dB. The output power P_{sub} carried by substrate modes (green squares in Fig. 2) was measured by laterally shifting the collecting fiber by about 50 μm from port C and is independent of the circuit layout.

The main result contained in Fig. 2 is that radiative coupling decreases versus g with a much slower scaling law than the exponentially decaying evanescent coupling. A numeric fit of the experimental data provides a power-law dependence of g^{-x}, with $x \simeq 2.8$. To support this finding, we developed a model to evaluate the expected optical crosstalk numerically in the two-waveguide system under consideration. Our model is based on the volume current method that was proved effective in predicting roughness-induced scattering losses in dielectric waveguides [9]. Roughness is considered a small perturbation of the dielectric constant profile of the waveguide and does not significantly alter the field pattern of the guided mode(s). With this assumption, the total field of the direct waveguide can be expressed as the superposition of an unperturbed guided mode pattern (primary field) and a (secondary) radiation field. As shown in Fig. 3, roughness is modeled as an array of dipoles located 300 nm (half the etch depth of the waveguide) above the interface between two half-spaces, the foreground and background media, with dielectric constants ϵ_f and ϵ_b, respectively. In the direct waveguide, dipoles are excited by the primary field and generate the secondary field. The current density $\mathbf{J}$ induced by the primary field $\mathbf{E}_i$ on a small volume element ΔV can be expressed as [9]

$$\mathbf{J} = j\omega(\epsilon_f - \epsilon_b)\mathbf{E}_i \tag{1}$$

and can be represented by an elementary radiating source (Rayleigh hypothesis) with a dipole moment $\mathbf{J}\Delta V$. We neglect mutual induction between dipoles on the same waveguide, so that the total scattered field is the sum of the fields due to all dipoles taken as if they were individually radiating. Likewise, the scattered field is collected by a second array of dipoles describing the roughness profile of the adjacent waveguide. Each dipole behaves like a point source with an induced dipole moment excited by the secondary field. This second dipole array produces a scattered field exciting both copropagating and counter-propagating modes in the adjacent waveguide. Radiative coupling is obtained by adding all the contributions in the same direction to the fundamental mode, even if, as discussed further on, a weak coupling to higher or leaky modes can occur. The computation is made faster by asymptotically evaluating Sommerfeld integrals for a half-space [10].

To simulate optical crosstalk in the structure of Fig. 1, we considered two 3-mm-long parallel dipole arrays placed at distance g. Within each array, dipoles are uniformly spaced at about 30 nm, comparable with the correlation length of the sidewall roughness [11]—the distance beyond which scattering events can be considered uncorrelated. Each dipole radiates independently with a random dipole moment distributed according to a zero-mean Gaussian probability density function. The dashed line in Fig. 2 shows the results obtained by averaging numerical simulations performed over the 1530–1570 nm wavelength range. For the considered structure and gap range, our model matches the experimental data well, providing as output a power-law dependence g^{-x} of the radiative crosstalk versus waveguide gap with the

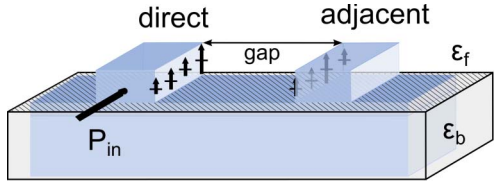

Fig. 3. Roughness on the two facing sidewalls is modeled by an equivalent array of dipole sources. Roughness on the other sidewalls is neglected.

same exponent $x = 2.8$ produced by the fit of the measurements. The model also shows that x is strongly related to waveguide geometry and index contrast. For instance, a simulation of channel waveguides buried in a homogeneous medium (e.g., silicon core surrounded by silica) provides a g^{-1} scaling law for optical crosstalk in agreement with predictions by Marcuse [12].

For deeper insight into the nature of crosstalk, we also investigated effects related to the excitation of higher order modes in the adjacent waveguide [13]. Figure 4(a) shows the measured crosstalk spectrum at port C of the device for different gaps. In the evanescent coupling regime ($g \leq 3$ μm), the coupled power P_{out} exhibits an almost flat spectrum with a small wavelength dependence, the slight increase with respect to the wavelength being due to the reduction of mode confinement in the waveguide, resulting in a higher field overlap of the coupled modes. Moving to larger gaps, spectral ripples appear and become more pronounced, reaching an amplitude of almost 10 dB for $g = 20$ and 30 μm. This behavior is consistent with a beating between the fundamental and the first higher order leaky mode inside the adjacent waveguide. Since the two modes have different propagation constants, the spatial distribution of the total field at port C periodically changes versus wavelength, leading to a different coupling efficiency with the collecting fiber.

The presence of higher order modes is confirmed by direct acquisition of the near field at the output ports of the device. We measured the field shape at both ports with an objective and a CCD camera. Figure 4(b) shows results for $g = 2$ μm and $g = 5$ μm at several wavelengths between 1540 and 1555 nm. As shown in the pictures, a normalization factor is used to obtain a better comparison of the spatial field distribution. In the evanescent coupling regime ($g = 2$ μm), the field shapes in the direct and adjacent waveguides are substantially identical at any wavelength. When the contribution of radiative coupling prevails ($g = 5$ μm), at port C, the shape of the field significantly changes with wavelength, providing clear evidence of the presence of more than one propagating mode in the adjacent waveguide with only the fundamental mode propagating in the direct waveguide (port B). These results show that optical crosstalk due to roughness-induced scattering can be responsible for the excitation of higher order leaky modes that can survive along the waveguide even though the waveguide is nominally single mode.

Finally, to obtain a full description of the optical crosstalk process, information on the phase of the field coupled to the adjacent waveguide is required. The phase relation between the optical fields propagating in the direct and adjacent waveguides was measured using coherent optical frequency domain reflectometry (OFDR) [5]. As shown in Fig. 5(a), in this experiment the test structure was conveniently reversed; port C was used as input waveguide and the reflected power was measured at the same port. Note that in this configuration, the role of direct and adjacent waveguide are mutually switched. The light reflected by the abrupt termination of the direct waveguide never crosses the coupling region and provides the reference phase ψ_d. On the contrary, the light reflected by the end facet of the adjacent waveguide (port A) and collected at port C crosses twice the coupling region and its phase ψ_a provides information on the phase shift associated with waveguide coupling.

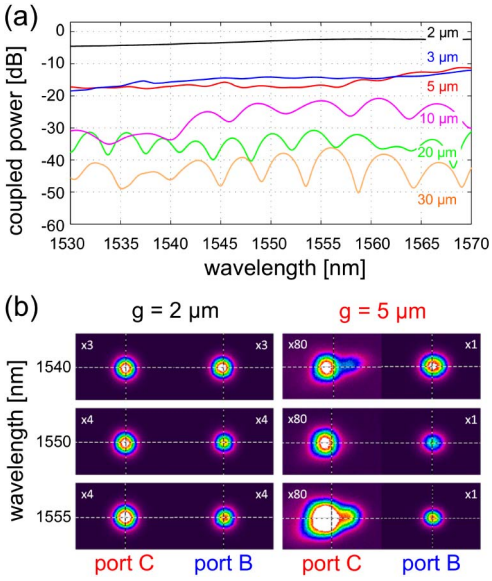

Fig. 4. (a) Normalized power spectral density $P_{\text{xt}}/\langle(P_{\text{out}} + P_{\text{xt}})\rangle$ measured for different values of the gap g. (b) Near-field measurements at the output ports B and C of the device for three wavelengths. For $g = 5$ μm, the effect of a multimode propagation appears.

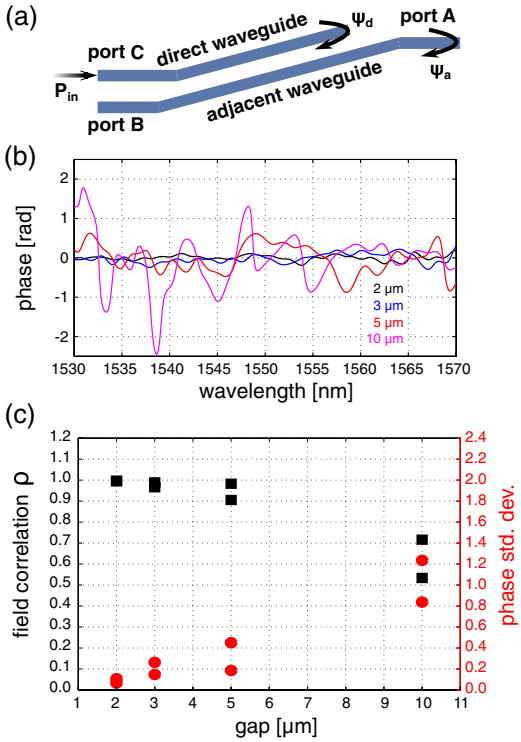

Fig. 5. (a) Schematic of the test structure for phase analysis. The phase ψ_d and ψ_a of the fields reflected at the end of both waveguides was measured at port C. (b) Measured spectral behavior of the phase difference $(\tilde{\psi}_d - \tilde{\psi}_a)$ compensates for propagation terms. Phase fluctuations increase for larger gaps confirmed in (c) by the increase of the standard deviation (red dots). Phase randomness in the coupled field causes fields decorrelation (black squares).

To compare ψ_a with ψ_d, the phase terms due to propagation along the waveguide sections were compensated through a quadratic dispersion model, taking into account first- and second-order waveguide dispersion. The compensated phases are given by $\tilde{\psi}_d = \psi_d - \widehat{\beta} L_d$ and $\tilde{\psi}_a = \psi_a - \widehat{\beta} L_a$, where L_d and L_a are the lengths of the direct and adjacent waveguides, respectively, and $\widehat{\beta}$ is the estimated propagation constant.

Figure 5(b) shows the phase difference $\Delta\psi = \tilde{\psi}_d - \tilde{\psi}_a$ for devices with increasing gap g from 2 to 10 μm in the 1530–1570 nm wavelength range. In the evanescent coupling regime ($g \leq 3$ μm), the spread of the phase difference $\Delta\psi$ is almost zero across the entire considered range, consistent with a coherent coupling mechanism that preserves the phase relation between exciting and coupled modes. For $g = 5$ μm, some ripples appear, indicating that $\tilde{\psi}_c$ contains an additional random contribution. This effect becomes more pronounced for $g = 10$ μm where the coupling mechanism is largely dominated by scattering induced radiation. As shown in Fig. 5(c) (red dots), the standard deviation of $\Delta\psi$, evaluated across the 40-nm-wide wavelength range for two sets of nominally identically devices, increases from almost 0 to more than 1 rad in the considered gap range.

The increase of the standard deviation of the phase spread $\Delta\psi$ suggests that the optical fields in the direct and adjacent waveguides progressively lose correlation when the gap distance increases. To provide a quantitative measurement of the correlation degree, we use the correlation coefficient

$$\rho = \frac{\sum_{i=1}^{N} (e_a - \langle e_a \rangle)(e_d - \langle e_d \rangle)}{\sqrt{\sum_{i=1}^{N} (e_a - \langle e_a \rangle)^2} \sqrt{\sum_{i=1}^{N} (e_d - \langle e_d \rangle)^2}}, \qquad (2)$$

where e_a and e_d are the complex amplitudes of the coupled and reference fields. For completely correlated signals, $|\rho| \to 1$; uncorrelated signals exhibit $|\rho| \to 0$. As shown in Fig. 5(c) (black squares), in the measured devices $|\rho|$ reduces from almost 1 (evanescent coupling) to about 0.6 when radiative coupling becomes the dominant crosstalk effect, confirming that the correlation of the field in the direct and adjacent waveguide decreases as the distance between the two waveguides increases.

In conclusion, optical crosstalk induced by sidewall roughness has been investigated and experimentally characterized. In a regime dominated by radiative contributions, a power-law dependence of the coupling on the gap between adjacent waveguides can be observed. This result is confirmed also by simulations performed through a model based on the volume current method. We also experimentally demonstrate higher order mode excitation as a consequence of radiative power coupling as well as decorrelation between exciting and coupled fields with increasing distance between the waveguides.

The authors gratefully acknowledge N. Groete, F. M. Soares, and M. Baier of the Heinrich Hertz Institute for the fabrication of the test samples. This work was partially supported by the European Community's Seventh Framework Programme FP7/2007-2013 under Grant ICT 257210 (PARADIGM).

References

1. J. Sun, E. Timurdogan, A. Yaacobi, E. S. Hosseini, and M. R. Watts, Nature **493**, 195 (2013).
2. W. Bogaerts, P. Dumon, D. V. Thourhout, and R. Baets, Opt. Lett. **32**, 2801 (2007).
3. J. Powelson, W. Feng, S. Lin, R. J. Feuerstein, and D. Tomic, J. Lightwave Technol. **16**, 2020 (1998).
4. G. Veronis and S. Fan, Opt. Express **16**, 2129 (2008).
5. F. Morichetti, A. Canciamilla, C. Ferrari, M. Torregiani, A. Melloni, and M. Martinelli, Phys. Rev. Lett. **104**, 033902 (2010).
6. D. Marcuse, Bell Syst. Tech. J. **50**, 1817 (1971).
7. D. Melati, F. Morichetti, A. Canciamilla, D. Roncelli, F. Soares, A. Bakker, and A. Melloni, J. Lightwave Technol. **30**, 3610 (2012).
8. A. S. Sudbo, J. Eur. Opt. Soc. A **2**, 211 (1993).
9. T. Barwicz and H. Haus, J. Lightwave Technol. **23**, 2719 (2005).
10. K. Michalski, IEE Proc. H **132**, 312 (1985).
11. W. Zhao, J. W. Bae, I. Adesida, and J. H. Jang, J. Vac. Sci. Technol. B **23**, 2041 (2005).
12. D. Marcuse, Bell Syst. Tech. J. **48**, 3233 (1969).
13. C. G. Poulton, C. Koos, M. Fujii, A. Pfrang, T. Schimmel, J. Leuthold, and W. Freude, IEEE J. Sel. Top. Quantum Electron. **12**, 1306 (2006).